JGR Space Physics

RESEARCH ARTICLE
10.1029/2019JA027314

Special Section:
Jupiter Midway Through the Juno Mission

Proton Acceleration by Io's Alfvénic Interaction

J. R. Szalay[1], F. Bagenal[2], F. Allegrini[3,4], B. Bonfond[5], G. Clark[6], J. E. P. Connerney[7,8], F. Crary[2], R. W. Ebert[3], R. E. Ergun[2], D. J. Gershman[8], P. C. Hinton[2], M. Imai[9], S. Janser[10], D. J. McComas[1], C. Paranicas[6], J. Saur[10], A. H. Sulaiman[9], M. F. Thomsen[11], R. J. Wilson[2], S. Bolton[3], and S. M. Levin[12]

[1]Department of Astrophysical Sciences, Princeton University, Princeton, NJ, USA, [2]Laboratory for Atmospheric and Space Physics, University of Colorado Boulder, Boulder, CO, USA, [3]Southwest Research Institute, San Antonio, TX, USA, [4]Department of Physics and Astronomy, University of Texas at San Antonio, San Antonio, TX, USA, [5]Space Sciences, Technologies and Astrophysics Research Institute, LPAP, Université de Liège, Liège, Belgium, [6]The Johns Hopkins University Applied Physics Laboratory, Laurel, MD, USA, [7]Space Research Corporation, Annapolis, MD, USA, [8]Goddard Space Flight Center, Greenbelt, MD, USA, [9]Department of Physics and Astronomy, University of Iowa, Iowa City, IA, USA, [10]Institute of Geophysics and Meteorology, University of Cologne, Cologne, Germany, [11]Planetary Science Institute, Tucson, AZ, USA, [12]Jet Propulsion Laboratory, Pasadena, CA, USA

Abstract The Jovian Auroral Distributions Experiment aboard Juno observed accelerated proton populations connected to Io's footprint tail aurora. While accelerated electron populations have been previously linked with Io's auroral footprint tail aurora, we present new evidence for proton acceleration due to Io's Alfvénic interaction with Jupiter's magnetosphere. Separate populations were accelerated above the Io torus and at high latitudes near Jupiter. The timing suggests the acceleration is due to Alfvén waves associated with Io's Main Alfvén Wing. The inferred high-latitude proton acceleration region spans 0.9–2.5 Jovian radii in altitude, comparable to the expected location for electron acceleration, and suggests the associated Alfvén waves are able to accelerate electrons and protons in similar locations. The proton populations magnetically connected to Io's orbit are recently perturbed, equilibrating with the nominal torus plasma population on a timescale smaller than Io's System III orbital period of ~13 h, likely due to wave-particle interactions. The tail populations are split into a wake-like structure with distinct inner and outer regions, where the inner region maps to an equatorial width nearly identical to the diameter of Io. The approximately symmetric surrounding outer regions are each slightly smaller than the central region and may be related to Io's atmospheric extent. The nominal, corotational torus proton population exhibits energization throughout all regions, peaking at the anti-Jovian flank of the inner core region mapping to Io's diameter. These proton observations suggest Alfvén waves are capable of accelerating protons in multiple locations and provide further evidence that Io's Alfvénic interaction is bifurcated.

Plain Language Summary The interaction between Jupiter's moon Io and Jupiter's rapidly rotating magnetic field produces a persistent aurora in Jupiter's upper atmosphere. The Juno spacecraft's trajectory crossed magnetic field lines connected to this aurora. We found that protons are accelerated in multiple places between Jupiter and Io. The interaction is evidenced in two distinct regions, with the central core region mapping to almost exactly the size of Io in the equatorial plane. We also find the protons that comprise the nominal "background" population are hotter in this central region.

Key Points:
- Three distinct populations of protons (10 eV to 50 keV) were observed connected to Io's auroral tail
- Alfvén waves accelerate protons both near the Io torus Alfvén boundary and at an altitude of 0.9–2.5 R_J
- Io's Alfvénic interaction is split into two regions spanning multiple Io diameters wide downtail

Correspondence to:
J. R. Szalay,
jszalay@princeton.edu

Citation:
Szalay, J. R., Bagenal, F., Allegrini, F., Bonfond, B., Clark, G., Connerney, J. E. P., et al. (2020). Proton acceleration by Io's Alfvénic interaction. *Journal of Geophysical Research: Space Physics*, *125*, e2019JA027314. https://doi.org/10.1029/2019JA027314

Received 17 AUG 2019
Accepted 20 DEC 2019
Accepted article online 27 DEC 2019

1. Introduction

Jupiter's moon Io generates one of the most persistent auroras in the solar system over radio (Bigg, 1964), infrared (Connerney et al., 1993; Connerney & Satoh, 2000), and ultraviolet wavelengths (Broadfoot et al., 1981; Clarke et al., 1996). Voyager measurements revealed that Io's relative motion of 57 km/s in the Jovian magnetosphere produces an Alfvénic disturbance (Belcher et al., 1981; Ness et al., 1979) that generates an Alfvén wave propagating away from Io toward Jupiter's polar regions (Acuña et al., 1981; Neubauer, 1980). As these Alfvén waves travel away from Io, they suffer partial or nearly complete reflection at plasma density gradients both in the Io torus and in the Jovian ionosphere (Gurnett & Goertz, 1981; Bagenal, 1983; Jacobsen et al., 2007; Hinton et al., 2019).

While many auroral features are generated at extended source regions in Jupiter's magnetosphere, Io's auroral footprint can be localized to a much more precise source region. Its auroral current system and

features encode key information regarding the moon's complex interaction with Jupiter's magnetosphere. Specifically, Io's auroral features include (1) a Main Alfvén Wing (MAW) spot (Bonfond et al., 2008; Saur et al., 2013) that is a direct byproduct of Io's interaction with the corotating plasma, (2) a transhemispheric electron beam spot that is interpreted to be a conjugate aurora related to the MAW on the opposite hemisphere, (3) a reflected Alfvén wing spot from multiple reflections within the Io torus, and (4) a long auroral tail trailing downstream of the MAW (see, for example, Figure 4 in Bonfond et al., 2008). In this study, we use the term "Io footprint tail" (IFPT) to describe Io's auroral tail in Jupiter's ionosphere.

Measurements from the Juno mission have shed light on the physical mechanisms behind these intense aurorae. Observations of broadband electron fluxes (Szalay et al., 2018) and direct measurements of associated Io-generated Alfvén waves (Gershman et al., 2019) suggest the IFPT is sustained by a predominantly Alfvénic acceleration mechanism (Bonfond et al., 2009, 2017; Crary & Bagenal, 1997; Jacobsen et al., 2007, 2010). Kinetic simulations of Alfvén waves generated in the Io torus have also found electron acceleration by dispersive scale Alfvén waves to be consistent with Juno observations (Damiano et al., 2019). Earth-based observations have indicated the presence of parallel potential structures capable of accelerating electrons on the order a few hundred electron volts (Hess et al., 2009). However, while parallel potential structures may also contribute to IFPT auroral acceleration (e.g., Delamere et al., 2003; Su et al., 2003; Hess et al., 2009; Ergun et al., 2009; Matsuda et al., 2012), in situ evidence to support a parallel acceleration scheme is lacking. Even beyond the IFPT, the predominance of Alfvénic acceleration at Jupiter compared to the more parallel potential-driven terrestrial aurora has been a major finding of the Juno mission (Mauk et al., 2017; Saur et al., 2018).

While Juno observations favor a primarily Alfvénic acceleration mechanism for the IFPT, the location and characteristics of the acceleration region(s) are still not fully resolved. Some studies point to an acceleration region inside the Io torus (Das & Ip, 1992; Crary, 1997), while others suggest a higher-latitude acceleration region (Jones & Su, 2008; Hess et al., 2010). Io-related acceleration of charged particles may also provide an additional energy source for the torus plasma populations (e.g., Tsuchiya et al., 2015), the extent of which is not well understood. The IFPT has also been observed to exhibit a split tail at least some of the time, both in plasma observations (Szalay et al., 2018) and in infrared images (Mura et al., 2018), but the nature of this dual tail has not been fully understood.

In this study, we present proton measurements acquired by the Jovian Auroral Distributions Experiment instrument (JADE, McComas et al., 2017) while connected to the IFPT at an angular separation of ~18° (System III longitude) from Io. Due to the relatively slow travel times of protons compared to electrons, the timing, energy, and pitch angles (PAs) of the observed proton populations support inferences regarding their acceleration source regions. In section 2, we first highlight the observation and orbital geometry of these measurements. In section 3, we discuss the proton observations as a function of anode and PA. Section 4 provides a discussion of the timing and location of associated Alfvén waves. In sections 5, we connect the observed proton populations to the IFPT. In section 6 we discuss our results in the larger context of Io's interaction with the Jovian magnetosphere, and we conclude in section 7 with a summary of our key points.

2. Observation Geometry

We focus on a unique measurement period that occurred during Juno's eighteenth perijove (PJ18), within a few minutes of the approximate central time of the feature, t_0 = 2019-043T14:59:20 (UTC). Unlike other transits of the IFPT by Juno, this transit occurred when the magnetic field was nearly parallel to Juno's spin axis. Due to the configuration of the JADE instrument, this allowed for nearly complete coverage of all ion PAs each time step. Figure 1 shows the geometry at this time in three separate reference frames. The left panel shows Jupiter's north polar projection, with Juno's footprint in black traced back to the 1-bar level with the JRM09 plus current sheet model (Connerney et al., 1981, 2018). Juno's trajectory footprint (locus of points traced along the magnetic field to the 1-bar surface in Jupiter's atmosphere) at t_0 is identified with the blue arrow. Also shown are footprints of Io throughout its orbit (solid gray line), the instantaneous MAW (gray dot), and the main oval (dashed gray line). The middle panel shows the Juno trajectory and the JRM09 field line connected to Juno at t_0 in a frame with the z axis parallel to Jupiter's magnetic

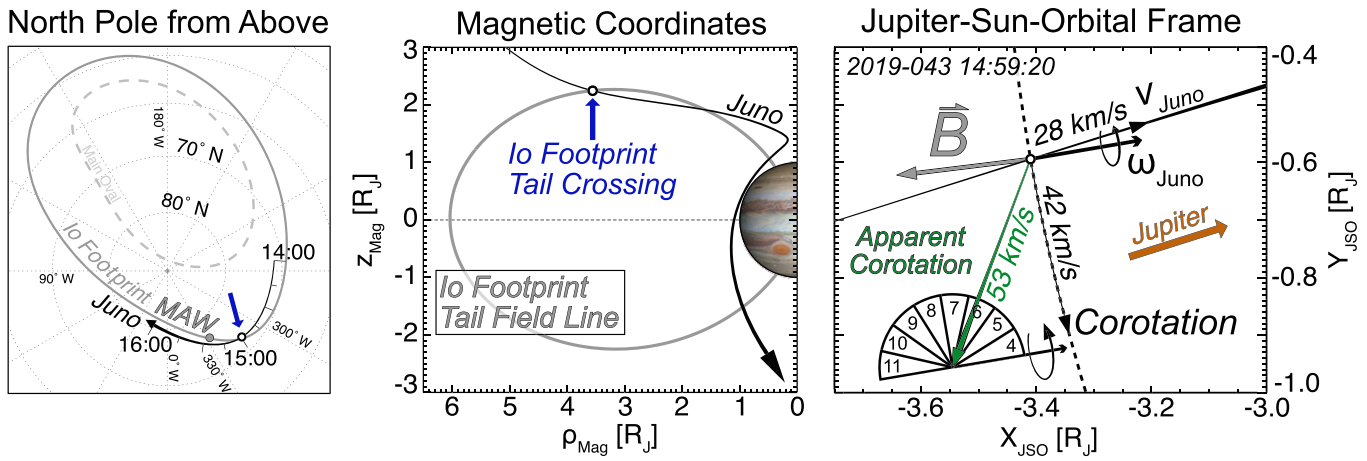

Figure 1. (left) View of the north pole from above in System III coordinates. The Juno trajectory mapped to the top of the Jovian atmosphere using the JRM09 model and the location of the Main Alfvén Wing (MAW). (middle) Trajectory in magnetic dipole coordinates. (right) Trajectory in JSO coordinates. Magnetic field, corotation, Juno speed, and Juno rotation axis vectors. The orientation of JADE anodes 4–11 are shown when approximately coplanar with the *X*-*Y* JSO plane.

dipole moment. During these observations, Io is displaced from the center of the torus southward by ~8° magnetic latitude.

The right panel of Figure 1 shows an expanded view of Juno's location in the Jupiter-Sun-Orbit (JSO, "Juno_JSO" in the NAIF/SPICE framework) *X*-*Y* plane, where the position of Juno at t_0 is indicated with the white dot. The magnetic field direction and Juno rotation axis are antiparallel within 5°. The field-of-view (FOV) for the JADE-I anodes 4–11 are shown at an instant the JADE-I detectors are all aligned with the *X*-*Y* plane. These detectors rotate about the rotation axis indicated in the figure, with Juno's rotational period of ~30 s. While higher-energy ions will be organized and detected across different detectors according to their PAs, the directionality of lower energy ions corotating with Jupiter will be influenced by the spacecraft's relative motion with respect to their trajectories as further described in Appendix A.

At t_0, Juno's Jovicentric speed is 28 km/s and local corotation is 42 km/s (at Juno's instantaneous position), as indicated by the arrows along the Juno trajectory and along the dotted line showing the corotation direction. Corotating ions will appear to come from the "apparent corotation" direction, the vector difference of the corotation velocity, and Juno's velocity, as indicated by the green vector with a magnitude of 53 km/s. Thermal plasma corotating with Jupiter's magnetic field lines will then be preferentially detected by the anodes most directly exposed to the apparent corotation direction, anodes 5–7.

3. Measurements

Here we focus on the proton measurements taken with the JADE ion instrument, JADE-I (McComas et al., 2017). This instrument measures ions in the range of 10 eV/Q to 46 keV/Q and has an instantaneous FOV of 270° × 90°, measuring ions over all directions in space each Juno spin period of ~30 s. JADE-I measures energy per charge; however, we use a specific mode that isolates protons from the other ion populations by including fluxes in the time-of-flight by energy space that correspond to protons, determined via laboratory calibrations. Therefore, we use units of energy instead of energy per charge as we can assume the protons have a single elementary unit of charge. The left portion of Figure 2 shows the JADE-I anodes along with their orientation to the local magnetic field and apparent corotation direction. The right portion of Figure 2 shows proton differential energy flux (DEF) for each of the eight anodes 4–11 for a duration of approximately 9 min of data centered around t_0. Anodes 0–3 are suppressed as they do not provide additional context, echoing their symmetric counterpart anodes 7–4, respectively. The time variations are all captured in anodes 4–11, and no apparent additional temporal information is gained by incorporating anodes 0–3. PAs are calculated with respect to the instantaneously measured on-board broadcasted magnetic field vector (Connerney et al., 2017). The proton populations observed are diverse, with different spatiotemporal variations observed across each anode.

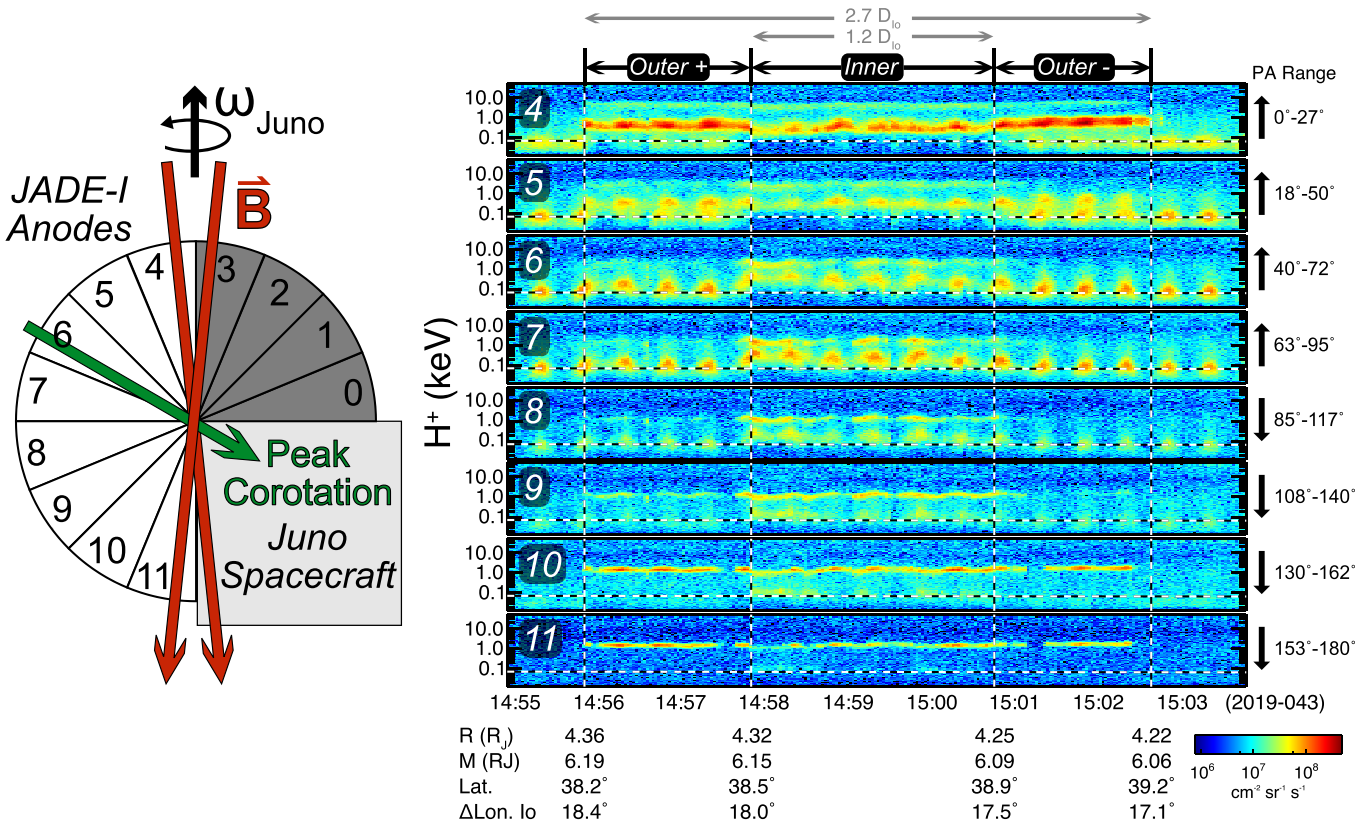

Figure 2. (left) JADE-I detector orientation with respect to the local magnetic field and apparent corotation direction. (right) Anodes 4–11 differential energy flux (DEF) spectrograms. The horizontal dashed line indicates the expected peak DEF for an equatorially picked up Maxwellian proton population flowing at the local corotation speed.

At the beginning and end of the time series, the unperturbed corotational Io torus proton population is observed. Assuming the corotational plasma is a Maxwellian distribution, the peak in the DEF will occur at

$$E_{\text{peak}} = \frac{m}{8}\left[v_p + \sqrt{v_p^2 + 8v_{\text{th}}^2}\right]^2 \quad (1)$$

where m is the ion mass, v_p is the local flow speed of the plasma with respect to the detector (apparent corotation velocity ~53 km/s), and v_{th} is the thermal speed of the Maxwellian. The peak in the DEF for a Maxwellian is derived by finding the peak in $E^2 f(v)$, where $f(v) \propto e^{-\left((v-v_p)/v_{\text{th}}\right)^2}$ is the distribution function as a function of particle velocity and $E^2 \propto v^4$. The horizontal dashed line in Figure 2 shows an approximate fit to the peaks of the pre- and post-IFPT encounter proton DEF, which is consistent with a Maxwellian drifting at the apparent corotation velocity of ~53 km/s and a temperature of ~20 eV. While not shown here, the derived temperature from the torus ion populations is related to the equatorial corotation energy and was previously observed for heavy ions at high latitudes (Szalay et al., 2017). We interpret this population as the unperturbed corotating torus with a local temperature ~20 eV. Following our assumption that this population is well represented by a Maxwellian distribution with sufficiently low energy its detection will preferentially occur on the anodes most exposed to the apparent corotation direction (see Appendix A for more details on low-energy PA anode dependence). As expected for such a population, the corotational torus plasma DEF peaks in anodes 5–7. The time variation in this population is due to the anode FOVs rotating into and out of the apparent corotation direction and the phase of this variation matches the expected FOV dependence.

We focus on the time period between 14:55:50 and 15:02:38 (2019-043), during which the corotational population is modified and accelerated. As highlighted on the top of the time series in Figure 2, the plasma

Table 1
Parameters at the Four Times Bounding Regions a–c

	2019-043	R	M	Lat.	ΔLon. Io	LC
Outer +	14:55:50	4.36 R_J	6.19 R_J	38.2°	18.4°	5.6°
Inner	14:57:47	4.32 R_J	6.15 R_J	38.5°	18.0°	5.6°
Outer -	15:00:45	4.25 R_J	6.09 R_J	38.9°	17.5°	5.8°
	15:02:38	4.22 R_J	6.06 R_J	39.2°	17.1°	5.9°

Note. R is radial distance from the center of Jupiter, *M* is the JRM09 magnetic *M*-shell, Lat. is the Jovian latitude, ΔLon. Io is the longitudinal separation between Io and Juno in System III coordinates, and LC is the JRM09 loss cone.

observations appear to be organized into two distinct regions: an inner region and symmetric outer region on the anti-Jovian side (Outer+) and Jovian side (Outer-), defined by characteristic changes in plasma populations in the DEF spectrograms. The "+" indicates the region on the anti-Jovian side, further from the planet. Table 1 lists the times of each boundary along with various parameters. The loss cone values in Table 1 are calculated using the JRM09 magnetic field model.

The Outer+ region is characterized by a modest energization of the corotational plasma, as shown by their peak energies displaced to a larger energy than the horizontal line indicating the expected corotational peak energy, most prominent in anodes 6 and 7. In addition, there are two new populations that are distinctly different than the corotational torus plasma. A primarily field-aligned population with a peak DEF energy of ~0.4 keV appears immediately at the onset of this region at 14:55:50. This population is most strongly observed in anode 4, which is the roughly field-aligned anode, covering a PA range of 0°–27°. The population appears quasi-periodic, as anode 4 oscillates within ~5° about the magnetic field direction. At Juno's location in the northern hemisphere, 0° PA corresponds to particles coming up the field line from Jupiter. Another population that is very narrow in energy appears with peak energies in the range of 1–4 keV across all anodes, with the highest fluxes in anodes 10–11 and a secondary peak in anode 4. The Outer− region is very similar to Outer+, both in total duration and characteristics of plasma populations observed, with the exception that the peak in the upward population DEF occurs ~0.6 keV. Mapping the field lines to Io's orbital plane to provide an Io-centric width determination, the width across regions Outer+ to Outer− is 2.7 D_{Io}. Here $D_{Io} = 2R_{Io}$ is the diameter of Io, where $R_{Io} = 1822$ km.

The inner region is characterized by an additional energization of the corotating torus population, which then decreases monotonically as a function of time for the remainder of the observations, most notable in the sharp jump of corotational peak energy in anodes 6–7 at 14:57:47, the boundary between Outer+ and the Inner region. Throughout the inner region, there is no longer any unperturbed corotational plasma. The peak energy of the primarily field aligned population is slightly decreased from ~0.4 to ~0.3 keV throughout this region. The narrow-energy population between 1 and 4 keV becomes more prominent in anodes 5–9. Mapping the field lines to Io's orbital plane, the width of the inner region is 1.2 D_{Io}. Figure 3 summarizes the three proton populations identified in the IFPT transit.

Figure 4 shows energy and PA spectrograms summed over anodes 4–11. The PA spectrogram is shown for all protons detected above 0.2 keV, the nonshaded region in the energy spectrogram. We show PAs for each 45°, twice the width of a single JADE-I anode (22.5°), to present a conservative calculation of the observed PA distribution. The region below 0.2 keV (<200 km/s) has been masked as this energy range is most susceptible to distortion of the measured energy and PAs due to the relative motion of the spacecraft with respect to the plasma flow speed. While the exact threshold to exclude the lower portion of the energy range from PA analysis is dependent on the phenomena of interest, a threshold of >0.2 keV ensures that the energy of the particles in the spacecraft frame are within a factor of 2 from the energy in the corotation frame for anode 6. This anode has a FOV that includes the apparent corotation direction and thus observes the corotational flow (Appendix A). The three populations are clearly delineated across mostly separate energy ranges.

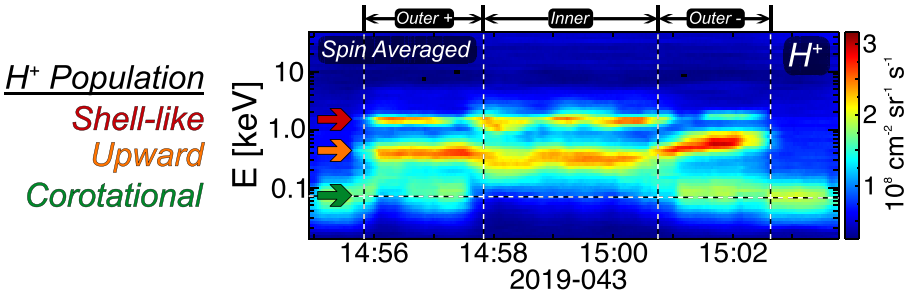

Figure 3. The three proton populations identified during the IFPT transit. Arrows and colored labels indicate the shell-like (red), upward (orange), and corotational (green) populations.

The bottom five panels show DEF as a function of parallel and perpendicular velocity in the spacecraft frame. Fluxes for energies less than 0.2 keV are masked out. There are eight PA wedges, directly corresponding to the anodes, with the upward top wedge showing anode 4 and the bottom downward wedge showing anode 11. Each wedge is shown with the angular width of the JADE-I anodes, 22.5°. Since the magnetic field is oriented within 5° of the Juno spin axis, each anode views a slightly expanded PA range throughout a single spin (noted on the side of Figure 2 for each anode). However, since the angular width of 22.5° of each anode is much larger than the magnetic offset of ±5°, we display each anode as mapping directly to PAs assuming the magnetic field was perfectly aligned with the spin axis. The predicted loss cone is ~6° (using JRM09) at Juno's location for this period, indicated with the gray wedges in Figure 4, which is consistent with the magnetic field offset from the spin axis, so the loss cone cannot be directly determined from these proton observations.

Before Outer+ and after Outer−, the velocity distributions are fairly uniform with low fluxes of the primary population above the 0.2 keV threshold we have adopted. In the outer regions, the ~0.3- to 0.6-keV population is prominent, peaking dominantly in the upward anode 4, corresponding to protons moving away from Jupiter. There is a slightly larger upward DEF in the Outer− region compared to Outer+, and the peak DEF energy varies from ~0.4 keV in Outer+ to ~0.6 keV in Outer−. Throughout the inner and outer regions, a "shell-like" population is present throughout all PAs from ~1 to 4 keV (440–880 km/s). We use the term "shell-like" as this population is similar to a shell distribution; however, the energy of the peak varies somewhat with PA. The largest fluxes of this population are observed in anode 10 in the PA range of 130–162° corresponding to protons traveling downward toward Jupiter. The coverage of greater than 22.5° in PA is due to the small offset angle between Juno's rotation axis and the magnetic field. In the inner region, the upward population has a smaller peak energy of ~0.3 keV (240 km/s) and is lower in flux compared to the outer regions. The shell-like population in the inner region is more uniform in flux across the eight PAs, with a peak still observed in anode 10. Throughout all regions, the downward flux detected in anodes 10–11 exhibits less temporal variation compared to the remaining shell-like fluxes across the other anodes, where the protons in the shell-like population peak in flux in the inner region and are reduced in the outer regions.

For completeness, we note that there was also a large enhancement of electrons below 10 keV observed by the JADE electron sensors during these times, where the span of the enhancement is exactly coincident with the period discussed here. However, during that time interval the electron sensors fields-of-view covered a PA range from ~60° to ~120° that limits our ability to make comprehensive comparisons with the proton data.

4. Alfvén Wave Propagation

To better understand whether these additional populations may be linked to Io's Alfvén wave system, we investigate how the timing of Alfvén wave propagation relates to these measurements. Figure 5 summarizes the configuration of the Alfvén wave system. The black line in Figure 5 shows the path that an Alfvén wave emitted at t_0 will take subsequently in System III longitude and latitude determined from the model of Hinton et al. (2019). In this model, Hinton et al. (2019) compared the location of the first few Io-Jupiter

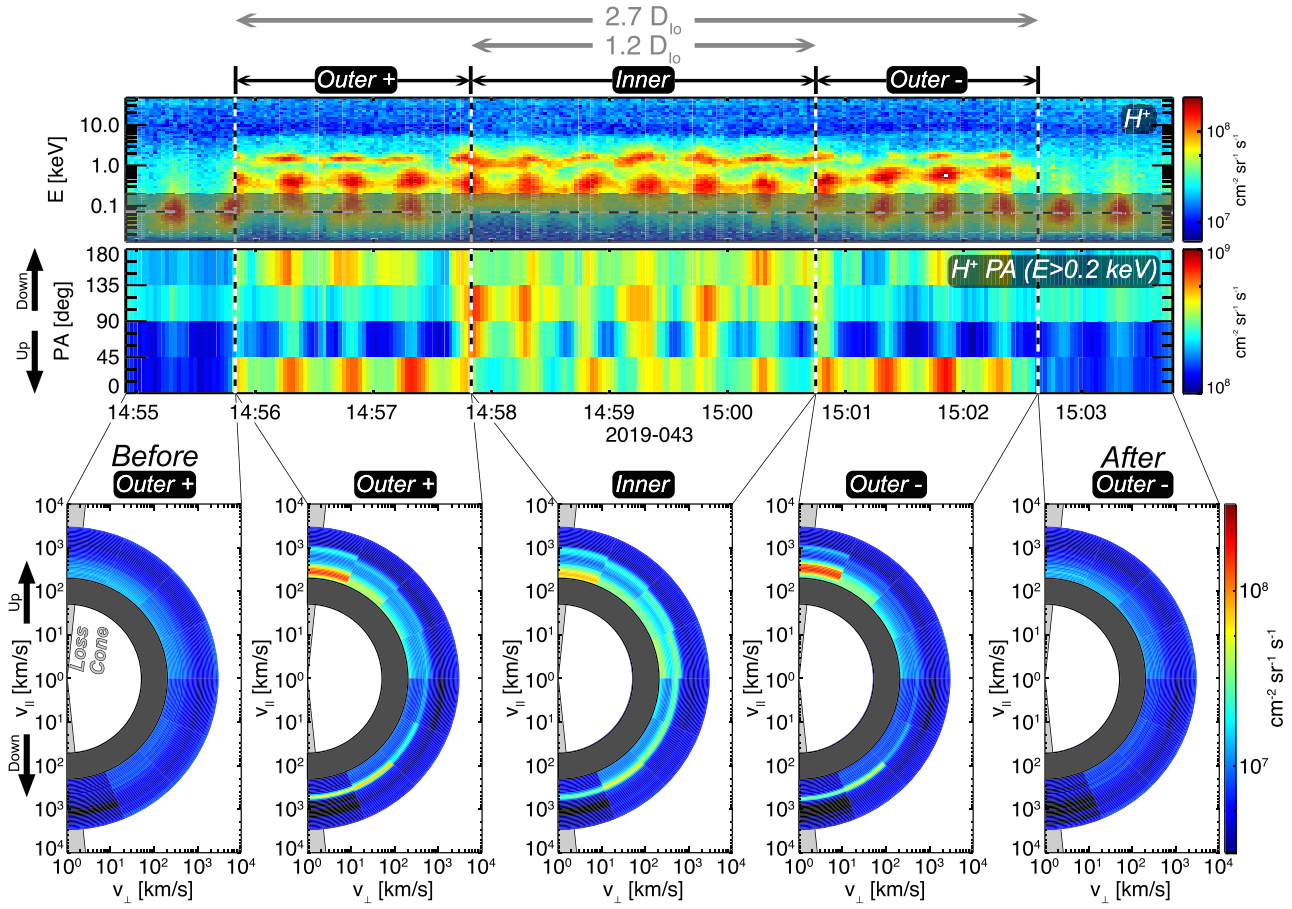

Figure 4. (top) JADE ion energy and pitch angle spectrograms for protons. (bottom) Differential energy flux in parallel versus perpendicular velocity space.

Alfvén bounces with Hubble Space Telescope (HST) observations of the Jovian aurora and found a consistent match, suggesting a reliable degree of accuracy in the position of the Alfven wave structures in the IFPT. This model uses Voyager 1 and Cassini data to constrain a 3D diffusive equilibrium model of the Io plasma torus along the JRM09 magnetic field model. Specifically, the model uses Voyager-based torus properties (electron density and temperature; abundances of S^+, S^{2+}, S^{3+}, O^+, O^{2+}, Na^+, and H^+ ions; and ion temperatures) from Bagenal et al. (2017) that are derived along the spacecraft trajectory and extrapolated along the magnetic field using multispecies diffusive equilibrium. Alfven waves launched by Io through the torus are simulated assuming that Io is continuously launching Alfven waves that reflect at Jupiter's ionosphere.

The solid line shows the Main Alfvén Wing, and the dotted line shows the initial portion of the first reflected Alfvén wave. Flux tubes for all regions are shown with the gray shapes in the center of each panel, along with the boundaries of these regions and Juno's trajectory with a small arrow. While not shown in this frame, Juno cuts the Io wake-connected flux tubes obliquely in a frame fixed to Io, such that Juno is further from Jupiter in the Outer+ region and closer in the Outer− region (Table 1).

Io's instantaneous position is shown with the black circle, separated by 18° in longitude from the magnetic field line connected to Juno at t_0. The Main Alfvén Waves launched from Io both northward and southward are shown along with the initial portion of their corresponding reflected Alfvén waves. As described in Hinton et al. (2019) and references therein, the Alfvén waves reflect at the Jovian ionosphere in this model. We define the point at which the Alfvén speed reaches 1% the speed of light, shown with dashed lines, as the "torus Alfvén boundary". This boundary corresponds to the approximate location where the planetward and antiplanetward Alfvén waves are expected to diverge (Hinton et al., 2019). During these observations, Io is more southward of the Io torus equator, as indicated by the boundaries being shifted northward in this

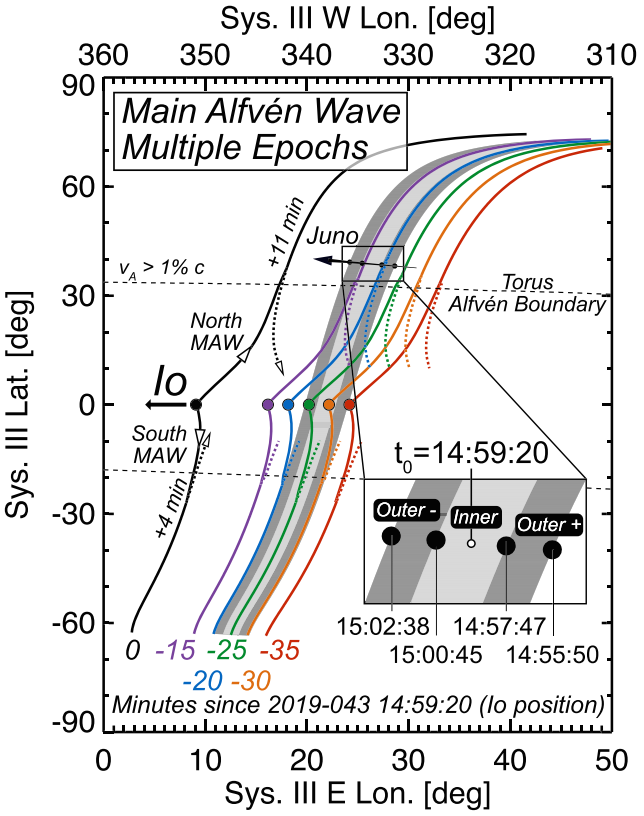

Figure 5. Alfvén bounce and timing dependence. The black line shows the Alfvén wave system launched at t_0. Additional colored lines show the Main Alfvén Waves launched at different epochs with respect to t_0, where the arrow indicates the direction of Io's relative motion and its length corresponds to the distance Io moves in 10 min. The dotted lines show the initial portion of the first reflected Alfvén waves.

coordinate system. In reality, the Alfvén waves may also partially reflect throughout the region between the torus and high latitudes with a sufficient plasma density gradient. Additionally, the reflection scheme shown here is idealized such that it does not include any nonlinear interactions that could play a role in geometry and intensity of multiple reflections (e.g., Jacobsen et al., 2007).

The timing of the Alfvén wave propagation, particularly the MAW, is critical to interpreting the proton observations. The Alfvén wave will always travel at the local Alfvén speed. The northern MAW takes ~11 min to reach the northern torus Alfvén boundary while the southern MAW takes a shorter time of ~4 min, since Io is lower in the torus during this observation. The MAW then travels at nearly the speed of light outside of the torus, reaching Jupiter's atmosphere within seconds of passing the torus Alfvén boundary. The reflected waves then transit back to the opposite hemisphere, taking approximately 14 min to reach the next torus Alfvén boundary. The labels on the black line of Figure 5 denote the time in minutes that it takes for the Alfvén waves reach the torus Alfvén boundaries after initially being launched from Io. The Alfvén waves shown in Figure 5 are therefore not a snapshot in time, rather they show the locations of Alfvén waves throughout their future evolution from being launched at Io to the initial portion of their reflection off the Jovian ionosphere.

Figure 5 also shows the MAW and a portion of the first reflected Alfvén wave that is initially launched at t_0 and 15, 20, 25, 30, and 35 min before t_0. As with the black line portraying the path the MAW would take after being launched at t_0, the traces along each Alfvén wave represent the path the wave will take after being generated at Io. Io's location is important as it constrains when any given field line is first exposed to the MAW. The inset shows relevant times for all regions. As shown here, Io had not yet reached the flux tubes connected to the inner/outer regions at 35 min before t_0. Io then reached the center of the inner region around 30 min before t_0. Since Io is southward in the torus, the southern MAW reaches the southern torus Alfvén boundary before the northern MAW reaches the northern torus Alfvén boundary. The southern MAW reaches the southern torus Alfvén boundary in the center of the inner region ~21 min before t_0, while the northern MAW reaches the northern torus Alfvén boundary in the center of the inner region ~6–7 min before t_0. Therefore, any proton acceleration that could have occurred at the Alfvén torus boundary due to the MAW would have been accelerated ~21 min before t_0 at the southern boundary and ~6–7 min before t_0 at the northern boundary.

5. Proton Populations

Having described the geometry and timing of the Io-generated Alfvén waves, we now seek to characterize the observed proton populations and determine the source regions of the accelerated shell-like and upward populations. We begin by describing the torus population and investigate its energization across the IFPT. For the shell-like and upward populations, we assume that after the protons are accelerated, they undergo motion conserving the first adiabatic invariant and are not further accelerated before being detected by JADE.

5.1. Corotational Torus Population

The nominal, corotational torus proton population is observed before and after the IFPT transit. We estimate the local proton temperature by relating the peak energy in JADE DEF spectrograms shown in Figure 2 to the thermal speed and invert equation (1) to solve for v_{th}. We assume this population can be approximated by a Maxwellian drifting at the local corotational velocity in the spacecraft frame. Additionally, any population of

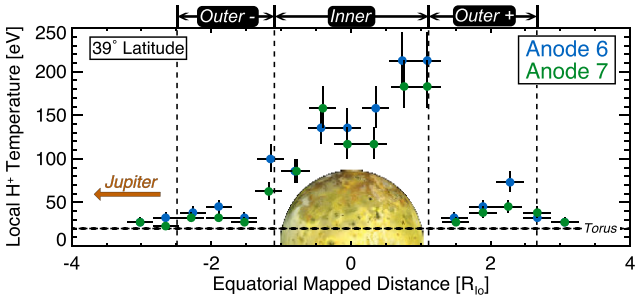

Figure 6. Estimates of the local proton temperature as a function of equatorial mapped distance.

equatorial plasma will exhibit a varying temperature anisotropy as a function of latitude (Crary et al., 1996; Huang & Birmingham, 1992). For example, the parallel temperature for a bi-Maxwellian plasma will remain constant along all latitudes, while the perpendicular temperature approaches the equatorial parallel temperature at high latitudes (Huang & Birmingham, 1992). Therefore, these calculations represent estimates of the local temperature and additional analysis must be performed to derive equatorial temperatures.

Figure 6 shows the estimated local proton temperatures derived from the peak DEF locations in anodes 6 and 7 as a function of distance mapped to the equatorial plane using the JRM09 model. Anodes 6 and 7 are chosen as they are the two anodes that best measure low-energy corotational protons. The distances given are relative and have been centered around the inner region. Before and after the IFPT transit, the temperatures are ~20 eV using $v_{th}^2 = 2k_BT/m$. These local temperature estimates are similar to equatorial torus proton temperatures of 50–80 eV derived from Voyager measurements (Bodisch et al., 2017); however, they are modified due to latitudinal anisotropy evolution as previously mentioned. Once Juno transits into the Outer+ region, the temperature increases to ~30–40 eV. There is a sharp transition between the Outer+ and inner regions, where the temperature jumps up to ~200 eV. This maps to the wake on Io's anti-Jovian flank and could be related to the interaction with Jupiter's magnetosphere and Io's atmosphere, where Io has a peak neutral density on the anti-Jovian flank (e.g., Jessup et al., 2004). It then decreases throughout the remainder of the inner and Outer− regions back toward the ~20 eV outside the Outer− region. There is a smaller local peak in both outer regions, further reflecting the symmetric character between the Outer+ and Outer− regions.

5.2. Shell-Like Population

To understand the shell-like population, we seek to determine if there could be a single source from which these protons may have originated. Due to PA and energy dispersion, a population of protons accelerated at a distant point on the field line may be detected across all PAs at another location. We first identify the peak DEF energy for each anode averaged over the inner region and assume that each anode is measuring particles with its center PA α, given in Table 2. We model the particles' motion backward in time from t_0 assuming they conserve the first adiabatic moment. Under this assumption, they gyrate on magnetic field lines and experience only the magnetic mirror force $F_\mu = -\mu\partial B/\partial s$, where $\mu = mv^2\sin^2\alpha/2B$ is the magnetic moment, m is the proton mass, v is the speed, α is the PA, B is the magnitude of the magnetic field, and s is the distance along the magnetic field line. The proton trajectories are integrated following their guiding center motion. We use the JRM09 magnetic field connected to Juno at t_0 for this simulation. Curvature and gradient drift are not included in this simulation. Since this integration occurs along a small number of bounces and during a small fraction of Jupiter's rotational period, these drifts do not appreciably modify the dynamics considered here.

Figure 7 shows the results of this simulation. The right panel is duplicated from Figure 4, where peak energies are indicated with color-coded dots that correspond to the time series data on the left of Figure 7, also given in Table 2. The eight colored lines correspond to the eight anodes, with anode 4 as dark red and anode 11 as dark blue. The time series shows the particles' motion as a function of time before they reached Juno at t_0, conserving the first adiabatic moment. The first panel shows their latitudes, along with horizontal lines for the location of the approximate latitude at which the MAW reaches the northern and southern torus Alfvén boundaries. The timing of the intersection of the MAW and torus Alfvén boundaries is determined by accounting for the travel time of Alfvén waves launched from a range of epochs and propagating to these boundaries (Hinton et al., 2019). The second panel shows east longitude along with the approximate longitude of the first northern and southern torus Alfvén reflection location. The third panel shows the distance to the southern torus Alfvén boundary. The fourth panel shows instantaneous PA.

Using this model, six of the eight trajectories from anodes 4–9 approximately converge in the southern hemisphere around 20 min before their detection, showing that it is possible that they originated from the same location and at the same time. Both the latitude and longitude at which they plausibly converge is almost

Table 2
Peak Energies and Pitch Angles (α) From the Inner Region in the Spacecraft Frame Used for the Particle Mirror Model

Anode	4	5	6	7	8	9	10	11
E_{peak}	3.9 keV	2.7 keV	2.3 keV	1.6 keV	1.4 keV	1.2 keV	1.6 keV	1.6 keV
α	12°	34°	56°	79°	101°	124°	146°	168°

exactly where the MAW is predicted to intersect the southern torus Alfvén boundary, indicated by the intersection of the trajectories with the dashed line. The convergence of these trajectories at ~20 min before detection at Juno is also shown by the absolute minimum in the third panel, where the majority of the protons are traced back almost exactly to the southern torus Alfvén boundary. This location approximately corresponds to the green Alfvén wave system in Figure 5 showing the Alfvén wave system launched 25 min before Juno's transit of these flux tubes (where the Alfvén wave reaches the boundary ~21 min before Juno's transit as it takes ~4 min for the Alfvén wave to reach the southern boundary). The 1.6-keV protons observed in anodes 10–11 do not converge at this point. These two populations also displayed characteristically different temporal behaviors, as they remained relatively constant in flux through all regions; the majority of the shell-like protons detected in anodes 4–9 exhibited a peak in the inner region, with lower fluxes in the outer regions.

If the majority of the protons in the shell-like population originated from a common source, these protons could have originated near the southern torus Alfvén boundary. If this is the case, such particles would have been accelerated northward once the MAW launched from Io reached the southern torus Alfvén boundary. They would have then transited the torus for about 10–15 min. The fastest protons (~2–4 keV) mirrored in the north and were observed by Juno in upward PAs as they were traveling away from their mirror points southward in the anti-Jupiter direction. The slower protons (~1–2 keV) took longer to travel the entirety of their path to Juno's location and were therefore detected as downward particles with PAs >90°, moving from the south toward Jupiter in the north. Therefore, a shell-like population with varying energies throughout PA space can originate from the same source, where the simultaneous detection of these particles at

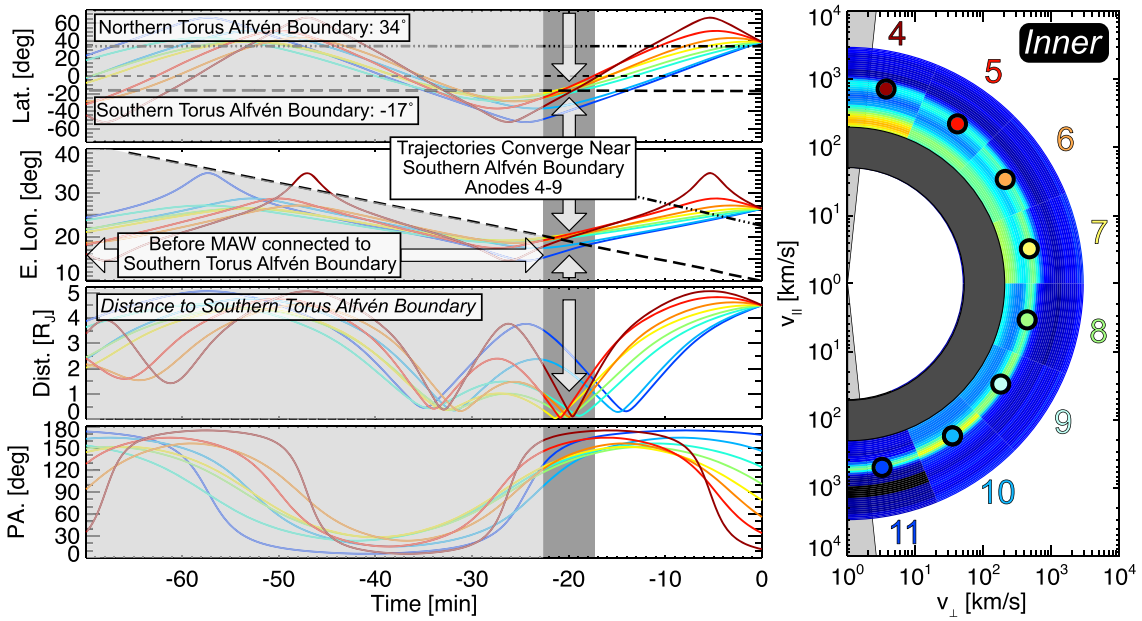

Figure 7. Simulating the "shell-like" population. The panels on the left correspond to latitude, System III east longitude, distance to the southern torus Alfvén boundary, and instantaneous pitch angle (PA) of the simulated particles. The dashed and dash-dotted lines indicate the predicted location of the intersection of the MAW at the southern and northern Alfvén torus boundaries, respectively. A horizontal short-dashed line indicates zero latitude. The light gray regions show times when the MAW had not yet reached the southern torus Alfvén boundary. The dark gray band indicates the approximate convergence time. The right panel is a replication from Figure 4.

different energies and PAs is due to velocity and PA dispersion. We note that additional transport effects could arise from magnetic field perturbations and scattering but do not consider those effects here. If the protons detected in anodes 4–9 were all accelerated at the same place and time, the protons observed in anodes 10–11 must have undergone a separate acceleration in a different location. The downward-going 1.4–keV protons observed in anodes 10 and 11 do not fit into the simple interpretation that they were accelerated at either of the reflection boundaries and not accelerated further after that.

If protons are accelerated at the southern torus Alfvén boundary, there should be a conjugate population of protons accelerated at the northern torus Alfvén boundary. However, the timing dictates whether or not Juno would be at the right combination of place and time for JADE to detect these protons. Juno is 0.6 R_J above the northern torus Alfvén boundary; therefore, 1.4- to 4-keV field-aligned protons take 0.8–1.4 min to travel from northern torus Alfvén boundary up to Juno's position at a latitude of 39°. Since the Alfvén wave reached the northern torus Alfvén boundary on Juno's t_0 field line Juno at 7 min before t_0, any population of downward going (traveling from the northern torus Alfvén boundary northward toward Jupiter) field-aligned 1.4- to 4-keV protons would have already transited past Juno's latitude of 39° approximately 6 min before Juno crossed the field line at t_0. If these particles are outside the loss cone, they would mirror and move southward. However, it would take them 10–20 min (depending on PA) to return to 39° latitude after mirroring. Therefore, Juno would also miss them as they would transit past 39° 4–14 min after t_0. Thus, Juno would be unable to measure a population of upward going 1.4- to 4-keV field-aligned protons accelerated at the northern torus Alfvén boundary due to the timing of the transit.

5.3. Upward Population

Similar analysis can be applied to the upward (up-going) population peaking at 0.3–0.6 keV in anode 4 in the DEF spectrogram. We assume this population was accelerated upward away from Jupiter at some location between the Juno spacecraft and Jupiter's northern atmosphere. Since the angular width of a single JADE-I anode is 22.5° and much larger than the loss cone of 6°, we cannot resolve the loss cone.

To estimate the source region the upward moving protons were accelerated, we determine where protons within a specific energy range would need to be accelerated away from Jupiter when the MAW transits across the field line to then reach Juno. For simplicity, we assume all protons are perfectly field aligned; this does not drastically affect the estimate on travel time to reach Juno if the protons have PAs less than the angular width of a single JADE-I anode (which this population is mostly restricted to). We then trace protons from Juno back in time until the MAW passes through the Juno-connected magnetic field line.

Figure 8 shows the travel time to reach Juno as a function of its position along the field line. The total distance along the field line from Jupiter's atmosphere to Juno at t_0 is ~3.7 R_J. Perfectly field aligned upward moving protons beginning right above the atmosphere with parallel energy in the range of 0.3–0.6 keV take 13–19 min to reach Juno, which is a maximum transit time since protons accelerated farther along the field line from Jupiter would take less time to reach Juno, as shown by Figure 8. As shown in Figure 5 (purple and blue curves), the MAW reaches the inner region ~4–9 min before t_0. As a conservative estimate, we use the full time range the MAW spanned the inner region to estimate the source region of the upward protons. Assuming this population was accelerated from the MAW, it would then be accelerated 4–9 min before t_0. The left panel of Figure 8 indicates the range of distances that a population of 0.3 to 0.6 keV protons could originate in this time. From this analysis, we estimate the source region of these upward going protons is at an altitude of 0.9–2.5 R_J along the field line.

Similarly, we can also estimate the location of the acceleration region throughout Juno's transit throughout the IFPT. The top right panel of Figure 8 shows the peak energy of the upward population in anode 4 for each Juno spin as a function of equatorial mapped distance. As with Figure 6, Jupiter is to the left and the horizontal axis is centered on the inner region. Vertical error bars indicate the FWHM of each peak. As before, we can infer the acceleration region according to the transit time and relative timing of the MAW along the field line connected to Juno at each time. We make the assumption that the spread in energy of the upward population is due to the acceleration region having a certain spatial extent and use the FWHM as a boundary on the acceleration region location. The bottom right panel of Figure 8 shows the derived acceleration regions for each spin. The centers of the features lie within our previous conservative estimate using t_0

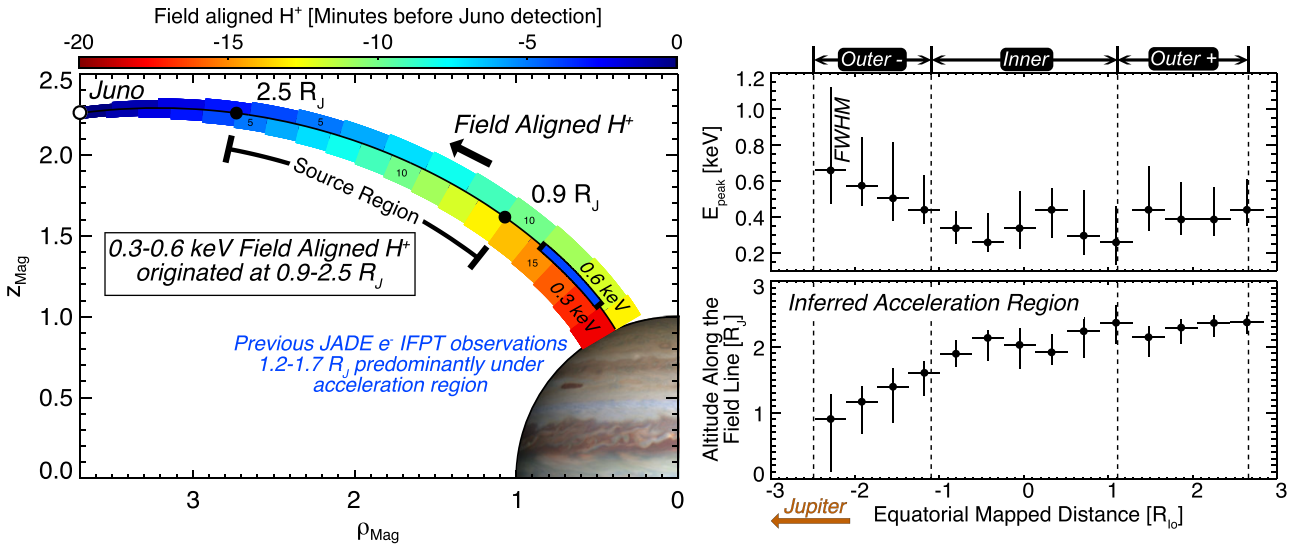

Figure 8. (left) Upward field-aligned travel time indicating the time a field-aligned 0.3 or 0.6 keV proton would take to reach Juno, with color indicating time. Assuming the protons were accelerated by the MAW, they were accelerated at within an altitude range of 0.9–2.5 R_J along the field line. (right) Peak energy and inferred altitude of the acceleration region. Horizontal and vertical error bars indicate one spin and FWHM from peak energy, respectively.

and a larger MAW time offset. These results suggest the acceleration region is closer to Jupiter in the Outer− region and increases in distance from Jupiter throughout the inner region, with a peak altitude of 2.0–2.4 R_J in the inner region. The acceleration distance is more uniform throughout the Outer+ region with an average altitude of ~2.3–2.5 R_J. The spatial extent/width of the acceleration region spans ~0.6 R_J on average along the field line, varying from 0.3 to 1.3 R_J throughout all regions.

6. Discussion

In the previous section, we assumed the shell-like and upward proton populations were accelerated at two separate source regions, did not encounter additional acceleration regions after initial acceleration, and conserved their magnetic moment throughout their transit along the magnetic field. With these assumptions and comparing to the timing and location of Io's Alfvén waves, we expect the shell-like population to have originated from the southern torus Alfvén boundary ~20 min before its observation and the upward population to have been accelerated between Juno and Jupiter's atmosphere in the altitude range of 0.9–2.5 R_J around ~7 min before its observation.

Figure 9 summarizes the observations discussed in this study. The spectrogram in the left panel shows a spin-averaged (30 s) version of the data from the top panel of Figure 4 in linear color scale. Three colored arrows indicate the three observed proton populations: corotational nominal torus (green), upward (orange), and shell-like (red). The top portion of the left panel in Figure 9 shows the inferred source regions for each of these three populations. Colored arrows near the Io torus Alfvén boundary (red) and near Jupiter (orange) show our expectations of approximately where these populations are accelerated. The middle panel shows a subset of the Alfvén waves responsible for accelerating these protons, along with the relative timing in minutes with respect to t_0.

We expect the nominal corotational torus protons are the source for the upward and shell-like populations. As shown in Figure 2, the nominal corotational torus population has a low temperature of ~20 eV (horizontal line) before and after the IFPT interaction. In anodes 5–7, where low-energy corotational plasma will be detected, this population is energized throughout all regions. This energization could be indicative of heating of the torus plasma population in the wake downstream of Io. If the entirety of the energization of the torus plasma is due to heating, it indicates that the temperature of the torus protons is enhanced from ~20 eV up to ~200 eV at the transition between the Outer+ and inner regions and monotonically decreases back to the nominal torus thermal speed by the end of the Outer− region. This temperature profile may be related to the hot pickup of Io's extended corona (Delamere et al.,

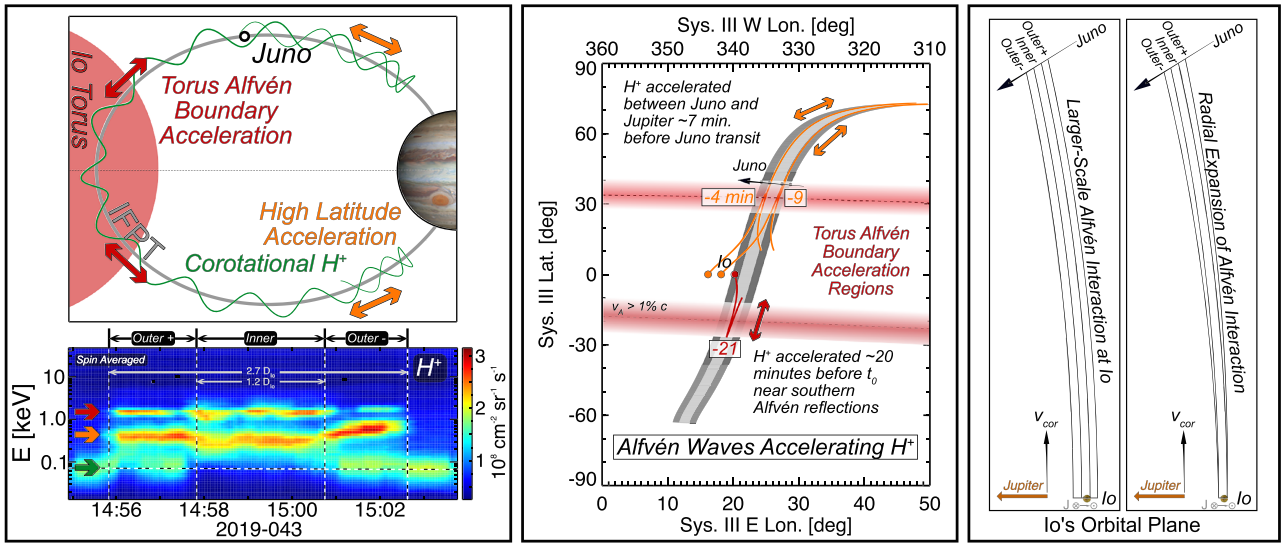

Figure 9. (left, top) Schematic showing the inferred acceleration regions. (left, bottom) The three proton populations observed. (middle) Alfvén waves responsible for the accelerated protons observed. (right) Schematic in Io's orbital plane showing two possible radial geometries of Io's Alfvenic interaction. An approximation of Juno's equatorially mapped trajectory along with inner and outer regions are shown at the top.

2003) and could indicate an asymmetric interaction between the magnetospheric plasma flow and Io, with a hotter pickup ion population on the anti-Jupiter hemisphere down the tail. Note that Juno does not observe the near-equatorially constrained particles, which most likely dominate the density in the torus. There is also no temperature depression mapped to the center of the wake as observed in Galileo measurements taken immediately downstream in Io's wake (Bagenal, 1997; Frank et al., 1996). The Juno measurements may be connected to a region in the wake that no longer has such a local temperature depression. More extensive analysis should be performed to investigate the origins of these energized torus protons, particularly if their local temperature anisotropy can be determined to better constrain the extent to which they are heated and/or accelerated.

The upward moving 0.3 to 0.6 keV protons were inferred to be accelerated in the range of 0.9–2.5 R_J altitude, as shown in Figure 8. If these protons are entirely in the loss cone and were to travel to the southern atmosphere, they carry an energy flux of ~0.5–2 mW/m^2. Therefore, they are not sufficient to produce IFPT aurora compared to the electron fluxes of ~10–100 mW/m^2 observed at similar longitudinal separations (Szalay et al., 2018). Also highlighted in Figure 8 with the blue segment of the field line is the range of IFPT JADE electron measurement locations taken during PJ5, PJ6, and PJ7 at longitudinal separations of ~10–120° down the tail. The majority of those observations suggested Juno was below the acceleration region, as the downward electron fluxes were 10–100 times larger than the upward fluxes. The exception to this was the PJ5 southern measurement that showed nearly equal fluxes of upward and downward electrons and was interpreted to be within the acceleration region. However, none of those measurements could constrain the spatial extent such an acceleration region would span along the field line.

Using the peak energy and FWHM of each spin, along with the timing of the predicted MAW, we estimate the location of the acceleration region throughout the IFPT transit (right panel of Figure 8). This relies on the assumption that changes in energy are directly related to dispersion such that larger peak energies in the upward population are interpreted to come from a source closer to Juno. The inferred location of the acceleration region follows a similar, asymmetric trend as the derived corotational temperature. The acceleration region is furthest from Jupiter at the transition between the Outer+ and inner regions, which maps to the anti-Jupiterward flank of Io's wake (right panel of Figure 9). While this could suggest the location of the acceleration region is dependent on the temperature of the corotational plasma population, there is minimal correlation in the Outer+ region between the location of the acceleration region and the temperature. Therefore, we cannot make a clear correlative or causal link in this analysis.

The inferred acceleration region altitude of 0.9–2.5 R_J is consistent with previous electron measurements and is also consistent with theoretical predictions of the peak parallel Alfvénic electric field magnitude. This peak electric field is predicted to occur at altitudes of 0.5–0.9 R_J, such that a large portion of the acceleration would occur above this altitude (Hess et al., 2010; Jones & Su, 2008). It is also consistent with kinetic simulations of dispersive scale Alfvén waves, which found these waves can lead to energization and acceleration of electrons at high latitudes above 0.5 R_J altitude (Damiano et al., 2019). The IFPT JADE observations now suggest that both electron and proton acceleration occur in similar regions along the IFPT flux tubes. If they are exactly coincident, proton observations could be used to quantitatively constrain the spatial extent of the acceleration region for electrons generating the IFPT aurora.

One possible energization mechanism for the observed upward proton population at low altitudes could be ion wave-particle interaction with kinetic Alfvén waves. In contrast to the generally assumed larger electron temperatures in the acceleration region of the Jovian main auroral oval (M~20–30), lower electron temperatures at $M = 6$ might provide a possible reason for significant damping of kinetic Alfvén waves at perpendicular scales smaller than the electron inertial length. Thus, not only electrons as in the case of the main auroral oval (Saur et al., 2018) but also protons might be subject to wave-particle interaction with kinetic Alfvén waves in the dilute plasma region at M-shell distances of Io. Further investigation of this hypothesis is outside the scope of this paper and will be subject of a future study. Additionally, the energy of the upward observed protons is similar to that of the electric potential jumps inferred by Earth-based radio emission observations of the Io-Jupiter flux tube (Hess et al., 2009). However, we favor an Alfvénic acceleration mechanism as an explanation for upward ion population given the increased importance of Alfvénic acceleration in the IFPT (Gershman et al., 2019; Szalay et al., 2018). While it is possible this population could have been accelerated by a transient parallel potential structure, JADE measurements of precipitating electrons do not support the existence of such a continually present potential structure spanning the footprint tail during Juno's transits through the auroral flux tubes (Szalay et al., 2018).

With respect to the other accelerated population, the majority of the shell-like protons were traced back to the torus Alfvén boundary in the southern hemisphere, where the backtracked proton trajectories from anodes 4–9 well coincide with the location of Io's southern MAW ~20 min before Juno's transit of the IFPT flux tubes. This location is approximate, as the source region is expected to have some latitudinal extent. The middle panel of Figure 9 shows the Alfvén wave system most likely responsible for accelerating this population in red. We note that the back-traced proton trajectories also converge at approximately 33 min before t_0. However, the MAW had not yet reached the field line connected to Juno at this time, indicated by the light gray region in Figure 7, hence any potential acceleration could not be driven by Io's MAW at this time. We therefore favor an initial acceleration time at ~20 min before t_0, given that the majority of back-traced trajectories converge at this point, which coincides with the location of the MAW at the southern torus Alfvén boundary.

The downward-going protons detected in anodes 10–11 in the shell-like population remained relatively constant in flux throughout Juno's transit through all regions, characteristically different than the other shell-like protons whose flux peaked in the inner region. They did not fit within the simple back-tracing model to coincide with the southern torus Alfvén boundary. Additionally, these protons did not fit into the trend in peak energy as a function of PA for the remaining shell-like DEF peaks, where the peak energy monotonically decreases from 3.9 keV at PA = 12° (anode 4) to 1.2 keV at PA = 124° (anode 9), shown in Table 2. If these protons did fit within the linear trend relating PA to peak energy, we would expect a peak in anodes 10 and 11 of 1.0 and 0.8 keV, respectively. Running the same simulation used for Figure 7 shows that with these energies, the protons do meet at the southern torus Alfvén boundary with the remaining protons. If these protons did originate with the other shell-like protons at the southern boundary, they would need to experience a subsequent parallel acceleration of ~0.8 keV near Juno to be consistent with the remaining shell-like protons. We note that shells at a finite energy are unstable and would expect wave generation due to this population. While another possibility for the generation of this population could be due to PA scattering of a proton beam, the spatiotemporal coincidence of back-tracing these protons to the Alfvén torus boundary leads us to favor the Alfvén torus boundary acceleration origin.

The two accelerated populations discussed in the study were accelerated in different hemispheres. The shell-like population appears to be accelerated at the southern torus Alfvén boundary, and the upward population appears to be accelerated in the high latitudes of the northern hemisphere. There is no reason to expect either these processes are exclusive to a given hemisphere, so we would expect a conjugate population for each to be accelerated in opposite hemispheres under similar conditions. Even without the specific MAW timing estimates constraining the source acceleration region to 0.9–2.5 R_J altitude, if the upward protons are accelerated between Juno and the planet, they must be accelerated above Juno's latitude of 39°. If such a conjugate population exists, we would expect the field lines to be populated with both upward and downward going protons from this acceleration. However, protons accelerated with purely parallel energies of 0.3–0.6 keV at lower than −39° latitude in the south would take at least 30–45 min to reach Juno. Therefore, such particles would not have reached Juno during its transit across all regions.

Similarly, for the shell-like population we would expect a population of protons to be accelerated at the northern torus Alfvén boundary. As previously discussed, the timing of the Juno transit would prevent the detection of a population of 1 to 4 keV protons accelerated by the MAW at the northern torus Alfvén boundary. These protons, if they exist, would have already passed Juno's position heading northward by the time Juno transited the field lines. Any particles 1–4 keV that are not in the loss cone would mirror and return back to 39° after Juno had already flown by. We therefore conclude that the absence of detection of conjugate populations from the most recent MAW transit is due to the timing of the Juno transit across these flux tubes.

The lack of detection of conjugates also suggests that any proton populations accelerated by Io's previous orbit had already equilibrated. This further reinforces the conclusion that these regions are not in steady state, rather they had only recently been disturbed by Io's Alfvénic interaction and were still being populated by various accelerated proton populations. These populations will then equilibrate over many bounces at a timescale smaller than Io's System III orbital period of $T_{\mathrm{Io,III}} = \left(T_{\mathrm{Io}}^{-1} - T_{\mathrm{Jup}}^{-1}\right)^{-1}$ ≈13 h, where $T_{\mathrm{Io}} = 42.5$ h and $T_{\mathrm{Jup}} = 9.9$ h are the Io's orbital period and Jupiter's rotational period, respectively. For example, the 0.3 to 0.6 keV upward population has an average bounce period of ~2 h. Therefore, this population must equilibrate within ~6.5 bounces or 13 incursions through the torus.

Coulomb collisions are not a significant factor of scattering for these protons. At the center of the torus, we estimate the timescale for energy loss from a 100 eV beam would be approximately 250 h (Huba, 2009; Nerney et al., 2017). Wave-particle interactions are, however, a plausible candidate for scattering on timescales well under 13 h. The observed distributions have a positive slope in phase space density and are therefore unstable. Determining the exact mode and growth rate of the instability is beyond the scope of the current study. In general, beam instabilities have growth rates related to the ion cyclotron, ion plasma, or lower hybrid frequencies. Of these, the ion cyclotron frequency is the lowest in the Io torus. We calculate that a 4 keV proton would traverse the torus (±20°) over a timescale on the order of 10^3 cyclotron periods and would pass through the torus about once every half hour. This provides ample time for wave growth and particle scattering in the 13 h implied by the data.

Additionally, while JADE observed specific energy ranges for the upward and shell-like populations, we cannot directly infer the initial distribution function of accelerated protons. Back-tracing the orbits conserving the first adiabatic invariant for the shell-like population, we expect the protons we detected had postacceleration PAs above ~120°, as shown in the bottom panel of Figure 7. This combination of energies and initial PAs at the boundary acceleration location was detectable by JADE due to the timing of the transit with respect to when the MAW passed by earlier. Hence, the range of energies detected is almost certainly a function of the timing of Juno's transit across the field lines previously connected to the MAW ~20 min beforehand.

For example, if there are protons accelerated at the torus Alfvén boundary with a factor of 10 higher in energy (10–40 keV), they would produce a similar shell-like distribution at 39° around 6 min after the MAW passed the southern torus Alfvén boundary (14 min before Juno arrived at this location). We therefore do not expect the detection of 1 to 4 keV shell-like protons to necessarily indicate a characteristic energy of the boundary acceleration process. Most likely it is a direct effect of the timing of the Juno transit. Transits

that occur nearer in time to the MAW boundary transits are expected to observe higher-energy shell-like proton populations, so long as the acceleration process is able to accelerate protons to higher energies than 4 keV. Similarly, the upward population may also include higher-energy protons that had already passed by 39° traveling southward before Juno arrived at this location. In a single pass, this makes reconstructing the full initial source distribution difficult. However, future studies could combine multiple passes occurring at different relative epochs to provide a more comprehensive understanding of the accelerated proton population near the acceleration region.

The accelerated proton populations discussed in this work have all been associated with the MAW. This is due to the fortuitous timing and location of Juno's transit across field lines connected to the IFPT during PJ18. We would also expect similar acceleration to occur at each successive instance of the reflected Alfvén waves further down the tail. However, the nature and timing of such accelerated protons may be complicated by nonlinear interactions of multiple Alfvén waves, whereby multiply reflected Alfvén waves may overlap and blend down the tail (Jacobsen et al., 2007). Since the MAW is mostly immune to these nonlinear effects due to it being the first instance of the Alfvén wave system, we do not consider nonlinear reflections in this study. Additionally, while outside the scope of this study, we would expect magnetic signatures to be present in Juno's magnetic field data linked to the regions identified in this study.

In addition to constraining the source of accelerated protons, these measurements provide unique insight into the radial structure of Io's Alfvénic interaction. The right panel of Figure 9 shows a schematic viewed from above Io's orbital plane. An approximate mapping of Juno's trajectory to Io's orbital plane is shown as well. The exact field line mapping from Juno's position to Io's orbital plane is not shown, as the small errors inherent in field line mapping can lead to absolute position errors with respect to Io. However, relative distances, such as the mapping distance across the various regions, are expected to be more accurate as they involve the difference of two mappings. While the Juno trajectory is a rough approximation, we capture the qualitative features of the orbit, where Juno's mapped equatorial field line moves from larger radial distances to smaller and from larger angular separations to smaller such that the Outer+ region is further from Io's instantaneous location than the Outer− region. The distances across all regions are shown to scale with respect to Io. In this panel, two different representations of Io's Alfvénic interaction are shown.

The equatorial width of the Outer+ and Outer− regions are 0.80 D_{Io} and 0.73 D_{Io}, respectively, with a total width of 2.7 D_{Io} across all regions. Juno's mapped field line is 36.7 D_{Io} and 34.9 D_{Io} down the tail in the equatorial plane for the Outer+ and Outer− regions, respectively. We envision two possible cases. Either Io's Alfvénic interaction region is approximately 3 D_{Io} and maintained down the tail or the interaction is roughly the size of Io and expands in the radial direction as it evolves down tail. The actual state of the tail could also be a combination of both cases. The angle subtended along Io's orbital path between the Outer+ and Outer− boundaries is ~1.2°. If there is radial expansion of the Alfvén system down the tail, using an azimuthal speed of 57 km/s, this corresponds to a radial expansion speed of ~1 km/s.

Previous work on the split tail signatures in the JADE electron observations somewhat favors the radial expansion scheme, where measurements of broadband electron distributions indicated widening as a function of angular separation from Io (Figure 9 in Szalay et al., 2018). The structure observed in the protons in this study is similar to the split tail electron observations. Of the first three PJs analyzed in the literature with JADE plasma data, PJ5 occurred when Io's MAW was ~10° from Juno's auroral footprint. Across the northern and southern transits of the IFPT, the total equatorial width of the feature was estimated to be 2–4 D_{Io} (Table 1 in Szalay et al., 2018). Of the six IFPT transits analyzed in that study, half of them showed evidence for a bifurcation in the auroral tail structure, with two peaks in the electron flux and a depletion between the two peaks. Additionally, infrared observations of the auroral emissions showed a split tail during a subset of observations (Mura et al., 2018).

As previously noted for the split features in the electron data (Szalay et al., 2018), the bifurcated structure could be related to the Alfvén wave intensity having a maximum on both flanks of Io (e.g., Jacobsen et al., 2007; Saur et al., 2013). The strength of the Alfvénic interaction depends on Io's atmospheric conductivity (e.g., Saur, 2004; Saur et al., 2013), and therefore, the extent of Alfvénically driven proton acceleration could encode key information on Io's atmosphere. For example, if the outer regions are related to Io's equatorial

flank atmosphere, auroral tail measurements could be used as a metric for Io's atmospheric extent and variability. With sufficient number of transits through the IFPT, auroral measurements could provide an additional pathway to constrain Io's atmospheric variations, either by sublimation or volcanic activity (e.g., Hue et al., 2019; Tsang et al., 2015). We note that plasma observations in the immediate plasma wake downstream of Io showed a double-peaked density structure across Io's wake (Bagenal, 1997). Additionally, at Saturn, split structures were also observed in Titan's plasma wake (e.g., Coates et al., 2007, 2012). If and how such density structures could be related to the split features in accelerated particles remains to be investigated.

Finally, these proton measurements indicate Io's Main Alfvén Wave has complex substructure, particularly with respect to particle acceleration. However, the substructure observed is a single snapshot during a transit across the IFPT and may not be fully representative of the MAW given the large variations in short angular distances observed in infrared emissions of the MAW and near-MAW tail (Mura et al., 2018). The inner region in this work is postulated to map directly to Io's wake and is highly asymmetric in the plasma signatures, both in the local torus population's temperature and the height of the inferred acceleration region. These observations along with the infrared observations of a highly structured tail may indicate a very nonuniform plasma environment in Io's wake (Mura et al., 2018). A cross-comparative study across multiple instruments would be critical to unfolding the relationship between Alfvénic substructure and Io's interaction with Jupiter's corotating plasma.

7. Conclusions

In this work, we present analysis on transient populations of protons connected to Io's footprint tail. These populations were most likely accelerated by Alfvén waves from Io's Main Alfvén Wing. Our results are summarized in the following key points.

1. Three distinct populations of protons are observed connected to Io's auroral tail. In addition to the expected nominal corotating torus protons, two new, unexpected populations were observed: a shell-like population 1–4 keV across all PAs and an upward 0.3- to 0.6-keV population moving away from Jupiter.
2. While Alfvén waves have been previously linked with electron acceleration in Io's footprint tail aurora at high latitudes, proton acceleration is observed to occur at similar altitudes of 0.9–2.5 R_J along IFPT flux tubes.
3. A new acceleration region is suggested to exist for protons at the Io torus Alfvén boundary.
4. Flux tubes connected to the IFPT are recently perturbed and relax in a timescale shorter than Io's System III orbital period of ~13 h, likely due to wave-particle interactions.
5. The nominal, corotational torus proton population exhibits energization throughout all three regions, peaking in the central core region mapping to Io's diameter.
6. Io's Alfvénic interaction is multiple Io diameters wide downtail, either due to a larger scale interaction at Io or radial expansion of the Alfvén wave/particle system.
7. Previous measurements of a split tail are further bolstered by the observation of symmetric regions on either side of Io's main Alfvénic interaction.

Appendix A: JADE-I PA and Energy Dependence

Determining the exact PA of ions measured by JADE is complicated by the relative motion of the spacecraft with those ions and Juno's spin phase. Here we focus on protons, and PA is defined in the corotational frame. When measuring protons that have a relative flow direction with respect to JADE, their apparent motion must be subtracted to calculate PA. As shown in the inset at the bottom right panel of Figure A1 (and shown in Figure 1), for the time range considered in this study Juno is moving 28 km/s toward Jupiter and the corotation direction is nearly perpendicular to its velocity vector with a corotation speed of 42 km/s. The apparent direction of corotation is $v_{app} = v_{cor} - v_{Juno}$, with a magnitude of 53 km/s and direction shown by green vector v_{app} in Figure A1.

First, let us consider the case in which the plane of the JADE anodes is identical to that of the plane containing v_{cor} and v_{Juno}, as illustrated in the bottom right panel of Figure A1. In this case, the apparent corotation

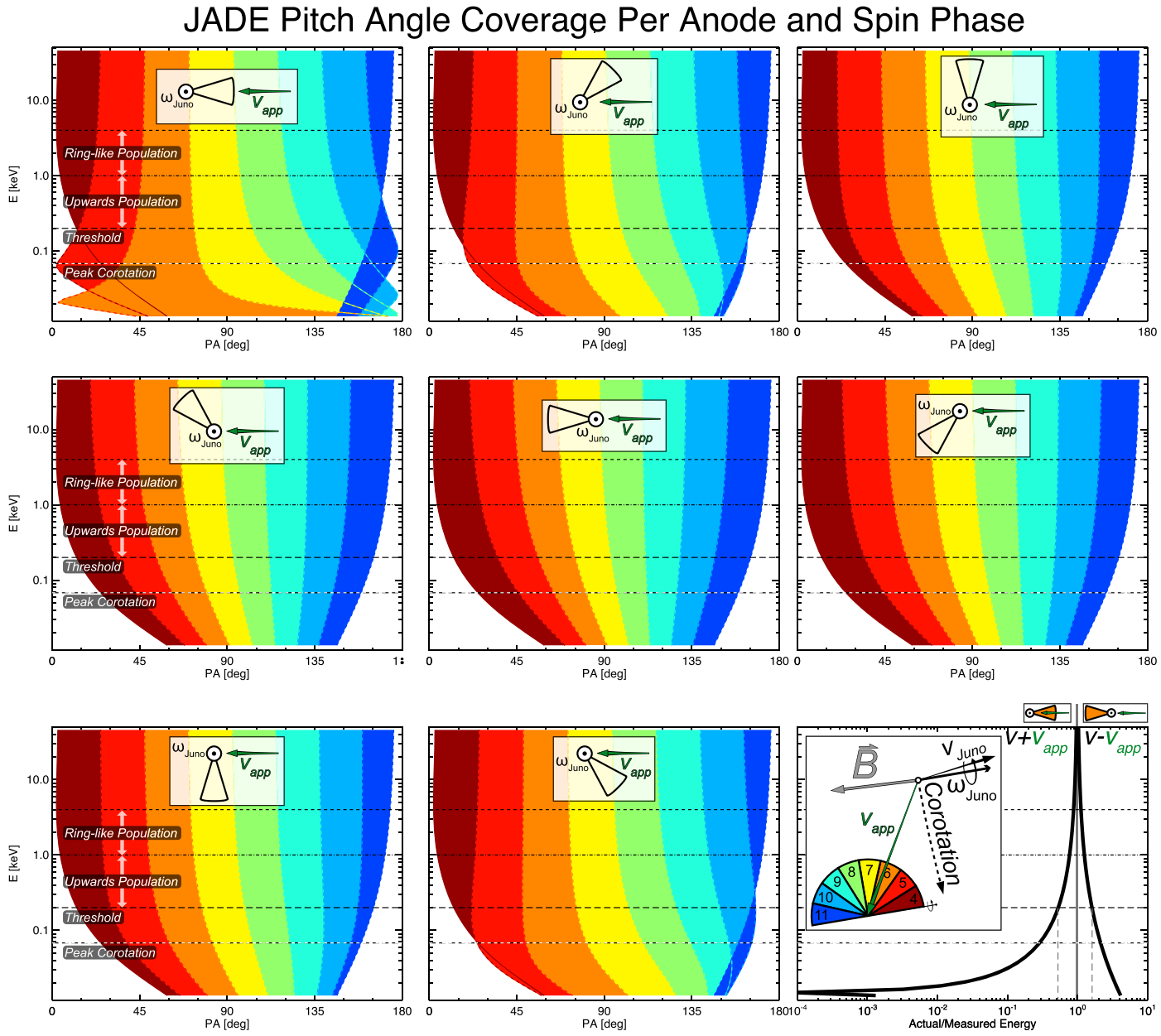

Figure A1. Pitch angle and energy dependence by anode.

vector impinges on anode 6. The top left panel of Figure A1 shows the anode that a proton will be detected in as a function of PA and measured energy for this specific spin phase. For very low energies in the corotational frame, protons will impact anode 6. Additionally, the measured energy is a function of the corotational energy and the apparent velocity. The bottom right panel of Figure A1 shows the ratio of energy as a function of actual/measured energy. The panel is split into two cases: one in which the apparent velocity vector is pointing into the JADE anodes (left) and when the JADE anodes have been rotated by 180°. When JADE is directly viewing the apparent corotation direction, the measured energy is greater than the energy of the particle in the corotating frame, due to the fact that Juno is "ramming" into the protons and adding their relative motion to the corotational frame energy. An extreme example occurs at energies near the apparent corotation energy. A proton with very low energy in the corotational frame will impact Juno with the apparent corotation speed of 53 km/s, which corresponds to 14 eV.

Therefore, the protons JADE measures as having 14 eV in anode 6 when this anode looks directly into the apparent corotation directions are actually very low energy protons in the corotating frame, as indicated by the very low value of actual/measured at this energy. For low-energy protons, anode 6 will "scoop" the majority of them up over a large range of PAs in specific spin phases.

Acknowledgments
The authors would like to thank the many Juno team members that made these observations possible. We thank V. Hue for producing the Juno footprint prediction times and locations. We thank two anonymous reviewers for their constructive feedback. The research was supported by NASA through Contract 699041X with SwRI. The JNO-J/SW-JAD-3-CALIBRATED-V1.0 data set was obtained from the Planetary Data System (PDS) at https://pds.nasa.gov/.

References

Acuña, M. H., Neubauer, F. M., & Ness, N. F. (1981). Standing Alfven wave current system at Io - Voyager 1 observations. *Journal of Geophysical Research*, *86*(A10), 8513–8521. http://doi.org/10.1029/JA086iA10p08513

Bagenal, F. (1983). Alfven wave propagation in the Io plasma torus. *Journal of Geophysical Research*, *88*(A4), 3013–3025. https://doi.org/10.1029/JA088iA04p03013

Bagenal, F. (1997). Ionization source near Io from Galileo wake data. *Geophysical Research Letters*, *24*(17), 2111–2114. http://doi.org/10.1029/97GL02052

Bagenal, F., Dougherty, L. P., Bodisch, K. M., Richardson, J. D., & Belcher, J. M. (2017). Survey of Voyager plasma science ions at Jupiter: 1. Analysis method. *Journal of Geophysical Research: Space Physics*, *122*, 8241–8256. https://doi.org/10.1002/2016JA023797

Belcher, J. W., Goertz, C. K., Sullivan, J. D., & Acuna, M. H. (1981). Plasma observations of the Alfven wave generated by Io. *Journal of Geophysical Research*, *86*(A10), 8508–8512. http://doi.org/10.1029/JA086iA10p08508

Bigg, E. K. (1964). Influence of the satellite Io on Jupiter's decametric emission. *Nature*, *203*(4949), 1008–1010. https://doi.org/10.1038/2031008a0

Bodisch, K. M., Dougherty, L. P., & Bagenal, F. (2017). Survey of Voyager plasma science ions at Jupiter: 3. Protons and minor ions. *Journal of Geophysical Research: Space Physics*, *122*, 8277–8294. http://doi.org/10.1002/2017JA024148

Bonfond, B., Grodent, D., Gérard, J.-C., Radioti, A., Dols, V., Delamere, P. A., & Clarke, J. T. (2009). The Io UV footprint: Location, inter-spot distances and tail vertical extent. *Journal of Geophysical Research*, *114*, A07224. https://doi.org/10.1029/2009JA014312

Bonfond, B., Grodent, D., Gérard, J.-C., Radioti, A., Saur, J., & Jacobsen, S. (2008). UV Io footprint leading spot: A key feature for understanding the UV Io footprint multiplicity? *Geophysical Research Letters*, *35*, L05107. https://doi.org/10.1029/2007GL032418

Bonfond, B., Saur, J., Grodent, D., Badman, S. V., Bisikalo, D., Shematovich, V., et al. (2017). The tails of the satellite auroral footprints at Jupiter. *Journal of Geophysical Research: Space Physics*, *122*, 7985–7996. https://doi.org/10.1002/2017JA024370

Broadfoot, A. L., Sandel, B. R., Shemansky, D. E., McConnell, J. C., Smith, G. R., Holberg, J. B., et al. (1981). Overview of the Voyager ultraviolet spectrometry results through Jupiter encounter. *Journal of Geophysical Research*, *86*(A10), 8259–8284. https://doi.org/10.1029/JA086iA10p08259

Clarke, J. T., Ballester, G. E., Trauger, J., Evans, R., Connerney, J. E. P., Stapelfeldt, K., et al. (1996). Far-ultraviolet imaging of Jupiter's aurora and the Io "footprint". *Science*, *274*(5286), 404–409. https://doi.org/10.1126/science.274.5286.404

Coates, A. J., Crary, F. J., Young, D. T., Szego, K., Arridge, C. S., Bebesi, Z., et al. (2007). Ionospheric electrons in Titan's tail: Plasma structure during the Cassini T9 encounter. *Geophysical Research Letters*, *34*, L24S05. http://doi.org/10.1029/2007GL030919

Coates, A. J., Wellbrock, A., Lewis, G. R., Arridge, C. S., Crary, F. J., Young, D. T., et al. (2012). Cassini in Titan's tail: CAPS observations of plasma escape. *Journal of Geophysical Research*, *117*, A05324. http://doi.org/10.1029/2012JA017595

Connerney, J. E. P., Açuna, M. H., & Ness, N. F. (1981). Modeling the Jovian current sheet and inner magnetosphere. *Journal of Geophysical Research*, *86*, 8370–8384.

Connerney, J. E. P., Baron, R., Satoh, T., & Owen, T. (1993). Images of Excited H_3^+ at the foot of the Io flux tube in Jupiter's atmosphere. *Science*, *262*(5136), 1035–1038. https://doi.org/10.1126/science.262.5136.1035

Connerney, J. E. P., Benn, M., Bjarno, J. B., Denver, T., Espley, J., Jorgensen, J. L., et al. (2017). The Juno magnetic field investigation. *Space Science Reviews*, *213*(1-4), 39–138. https://doi.org/10.1007/s11214-017-0334-z

Connerney, J. E. P., Kotsiaros, S., Oliversen, R. J., Espley, J. R., Joergensen, J. L., Joergensen, P. S., et al. (2018). A new model of Jupiter's magnetic field from Juno's first nine orbits. *Geophysical Research Letters*, *45*, 2590–2596. https://doi.org/10.1002/2018GL077312

Connerney, J. E. P., & Satoh, T. (2000). The H_3+ ion: A remote diagnostic of the Jovian magnetosphere. *Philosophical Transactions of the Royal Society of London - A*, *358*, 2471–2483.

Crary, F. J. (1997). On the generation of an electron beam by Io. *Journal of Geophysical Research*, *102*(A), 37–50. https://doi.org/10.1029/96JA02409

Crary, F. J., & Bagenal, F. (1997). Coupling the plasma interaction at Io to Jupiter. *Geophysical Research Letters*, *24*(17), 2135–2138. http://doi.org/10.1029/97GL02248

Crary, F. J., Bagenal, F., Ansher, J. A., Gurnett, D. A., & Kurth, W. S. (1996). Anisotropy and proton density in the Io plasma torus derived from whistler wave dispersion. *Journal of Geophysical Research*, *101*(A), 2699–2706. http://doi.org/10.1029/95JA02212

Damiano, P. A., Delamere, P. A., Stauffer, B., Ng, C.-S., & Johnson, J. R. (2019). Kinetic simulations of electron acceleration by dispersive scale Alfvén waves in Jupiter's magnetosphere. *Geophysical Research Letters*, *46*, 3043–3051. https://doi.org/10.1029/2018GL081219

Das, A. C., & Ip, W. H. (1992). Particle acceleration by kinetic Alfven waves in the Io plasma torus. *Planetary and Space Science*, *40*(11), 1499–1502. https://doi.org/10.1016/0032-0633(92)90046-Q

Delamere, P. A., Bagenal, F., Ergun, R. E., & Su, Y. J. (2003). Momentum transfer between the Io plasma wake and Jupiter's ionosphere. *Journal of Geophysical Research*, *108*(A), 1241. https://doi.org/10.1029/2002JA009530

Ergun, R. E., Ray, L. C., Delamere, P. A., Bagenal, F., Dols, V., & Su, Y. J. (2009). Generation of parallel electric fields in the Jupiter-Io torus wake region. *Journal of Geophysical Research*, *114*, A05201. https://doi.org/10.1029/2008JA013968

Frank, L. A., Paterson, W. R., Ackerson, K. L., Vasyliunas, V. M., Coroniti, F. V., & Bolton, S. J. (1996). Plasma observations at Io with the Galileo spacecraft. *Science*, *274*(5286), 394–395. https://doi.org/10.1126/science.274.5286.394

Gershman, D. J., Connerney, J. E. P., Kotsiaros, S., DiBraccio, G. A., Martos, Y. M., Viñas, A. F., et al. (2019). Alfvénic fluctuations associated with Jupiter's auroral emissions. *Geophysical Research Letters*, *46*, 7157–7165. https://doi.org/10.1029/2019GL082951

Gurnett, D. A., & Goertz, C. K. (1981). Multiple Alfven wave reflections excited by Io Origin of the Jovian decametric arcs. *Journal of Geophysical Research*, *86*(A2), 717–722. https://doi.org/10.1029/JA086iA02p00717

Hess, S. L. G., Delamere, P., Dols, V., Bonfond, B., & SwIFPT, D. (2010). Power transmission and particle acceleration along the Io flux tube. *Journal of Geophysical Research*, *115*, A06205. https://doi.org/10.1029/2009JA014928

Hess, S. L. G., Zarka, P., Mottez, F., & Ryabov, V. B. (2009). Electric potential jumps in the Io-Jupiter flux tube. *Planetary and Space Science*, *57*(1), 23–33. http://doi.org/10.1016/j.pss.2008.10.006

Hinton, P. C., Bagenal, F., & Bonfond, B. (2019). Alfvén wave propagation in the Io plasma torus. *Geophysical Research Letters*, *46*, 1242–1249. https://doi.org/10.1029/2018GL081472

Huang, T. S., & Birmingham, T. J. (1992). The polarization electric field and its effects in an anisotropic rotating magnetospheric plasma. *Journal of Geophysical Research*, *97*(1511), 1992.

Huba, J. D. (2009). *NRF Plasma Formulary* (pp. 31–33). Washington, DC: Naval Research Laboratory.

Hue, V., Greathouse, T. K., Bonfond, B., Saur, J., Gladstone, G. R., Roth, L., et al. (2019). Juno-UVS observation of the Io footprint during solar eclipse. *Journal of Geophysical Research: Space Physics*, *124*, 5184–5199. https://doi.org/10.1029/2018JA026431

Jacobsen, S., Neubauer, F. M., Saur, J., & Schilling, N. (2007). Io's nonlinear MHD-wave field in the heterogeneous Jovian magnetosphere. *Geophysical Research Letters*, *34*, L10202. https://doi.org/10.1029/2006GL029187

Jacobsen, S., Saur, J., Neubauer, F. M., Bonfond, B., Gérard, J. C., & Grodent, D. (2010). Location and spatial shape of electron beams in Io's wake. *Journal of Geophysical Research*, *115*, A04205. https://doi.org/10.1029/2009JA014753

Jessup, K. L., Spencer, J. R., Ballester, G. E., Howell, R. R., Roesler, F., Vigel, M., & Yelle, R. (2004). The atmospheric signature of Io's Prometheus plume and anti-Jovian hemisphere: Evidence for a sublimation atmosphere. *Icarus*, *169*(1), 197–215.

Jones, S. T., & Su, Y. J. (2008). Role of dispersive Alfvén waves in generating parallel electric fields along the Io-Jupiter fluxtube. *Journal of Geophysical Research*, *113*. https://doi.org/10.1029/2008JA013512

Matsuda, K., Terada, N., Katoh, Y., & Misawa, H. (2012). A simulation study of the current-voltage relationship of the Io tail aurora. *Journal of Geophysical Research*, *117*, A10214. http://doi.org/10.1029/2012JA017790

Mauk, B., Haggerty, D. K., Paranicas, C., Clark, G., Kollmann, P., Rymer, A. M., et al. (2017). Discrete and broadband electron acceleration in Jupiter's powerful aurora. *Nature*, *549*(7670), 66–69. https://doi.org/10.1038/nature23648

McComas, D. J., Alexander, N., Allegrini, F., Bagenal, F., Beebe, C., Clark, G., et al. (2017). The Jovian auroral distributions experiment (JADE) on the Juno mission to Jupiter. *Space Science Reviews*, Online first, *213*(1-4), 547–643. https://doi.org/10.1007/s11214-013-9990-9

Mura, A., Adriani, A., Connerney, J. E. P., Bolton, S., Altieri, F., Bagenal, F., et al. (2018). Juno observations of spot structures and a split tail in Io-induced aurorae on Jupiter. *Science*, *361*(6404), 774–777. http://doi.org/10.1126/science.aat1450

Nerney, E. G., Bagenal, F., & Steffl, A. J. (2017). Io plasma torus ion composition: Voyager, Galileo, and Cassini. *Journal of Geophysical Research: Space Physics*, *122*, 727–744. https://doi.org/10.1002/2016JA023306

Ness, N. F., Acuña, M. H., Lepping, R. P., Burlaga, L. F., Behannon, K. W., & Neubaur, F. M. (1979). Magnetic field studies at Jupiter by Voyager 1: Preliminary results. *Science*, *204*(4396), 982–987. https://doi.org/10.1126/science.204.4396.982

Neubauer, F. M. (1980). Nonlinear standing Alfven wave current system at Io—Theory. *Journal of Geophysical Research*, *85*(A3), 1171–1178. http://doi.org/10.1029/JA085iA03p01171

Saur, J. (2004). A model of Io's local electric field for a combined Alfvénic and unipolar inductor far-field coupling. *Journal of Geophysical Research*, *109*, A01210. https://doi.org/10.1029/2002JA009354

Saur, J., Grambusch, T., Duling, S., Neubauer, F. M., & Simon, S. (2013). Energy fluxes in sub-Alfvénic planet star and moon planet interactions. *Astronomy and Astrophysics*, *552*, A119. https://doi.org/10.1051/0004-6361/201118179

Saur, J., Janser, S., Schreiner, A., Clark, G., Mauk, B. H., Kollmann, P., et al. (2018). Wave-particle interaction of Alfvén waves in Jupiter's magnetosphere: Auroral and magnetospheric particle acceleration. *Journal of Geophysical Research: Space Physics*, *123*, 9560–9573. https://doi.org/10.1029/2018JA025948

Su, Y.-J., Ergun, R. E., Bagenal, F., & Delamere, P. A. (2003). Io-related Jovian auroral arcs: Modeling parallel electric fields. *Journal of Geophysical Research*, *108*(A), 1094. https://doi.org/10.1029/2002JA009247

Szalay, J. R., Allegrini, F., Bagenal, F., Bolton, S., Clark, G., Connerney, J. E. P., et al. (2017). Plasma measurements in the Jovian polar region with Juno/JADE. *Geophysical Research Letters*, *44*, 7122–7130. http://doi.org/10.1002/2017GL072837

Szalay, J. R., Bonfond, B., Allegrini, F., Bagenal, F., Bolton, S., Clark, G., et al. (2018). In situ observations connected to the Io footprint tail aurora. *Journal of Geophysical Research: Planets*, *123*, 3061–3077. https://doi.org/10.1029/2018JE005752

Tsang, C. C. C., Spencer, J. R., & Jessup, K. L. (2015). Non-detection of post-eclipse changes in Io's Jupiter-facing atmosphere: Evidence for volcanic support? *Icarus*, *248*, 243–253. https://doi.org/10.1016/j.icarus.2014.10.033

Tsuchiya, F., Kagitani, M., Yoshioka, K., Kimura, T., Murakami, G., Yamazaki, A., et al. (2015). Local electron heating in the Io plasma torus associated with Io from HISAKI satellite observation. *Journal of Geophysical Research: Space Physics*, *120*, 10,317–10,333. http://doi.org/10.1002/2015JA021420